Nonlinear Dyn (2022) 108:3693–3709
https://doi.org/10.1007/s11071-022-07434-2

ORIGINAL PAPER

Neural-based formation control of uncertain multi-agent systems with actuator saturation

Yang Fei · **Peng Shi** · **Cheng-Chew Lim**

Received: 25 October 2021 / Accepted: 1 April 2022 / Published online: 16 April 2022

Abstract The formation control problem for a group of first-order agents with model uncertainty and actuator saturation is investigated in this manuscript. An algorithm-and-observer-based formation controller is developed to ensure the semi-global boundedness of the formation tracking error with actuator saturation. First, a fully local-error-related cooperative weight tuning procedure is proposed for the adaptive uncertainty estimation of each agent. The effect of actuator saturation on both the cooperative adaptive estimation and the controller design part is then analysed and discussed. A three-layer neural-based observer is further constructed to achieve finite-time uncertainty approximation with actuator saturation. Besides, the reverse effect led by coupled and saturated control inputs is defined and a new control input distribution algorithm is presented to attenuate the potential oscillation in system states. Finally, comparative simulations based on a multiple omnidirectional robot system are conducted to illustrate the performance of the proposed formation controllers and the new algorithm.

Y. Fei · P. Shi (✉) · C.C. Lim
School of Electrical and Electronic Engineering, The University of Adelaide, Adelaide, SA 5005, Australia
e-mail: peng.shi@adelaide.edu.au

Y. Fei
e-mail: y.fei@adelaide.edu.au

C.C. Lim
e-mail: cheng.lim@adelaide.edu.au

Keywords Multi-agent systems · Actuator saturation · Three-layer neural networks · Formation control · Finite-time observer

1 Introduction

Recently, the cooperative control issue of multi-agent systems has become one popular research area in control engineering and robotics [2,16,17,26,27,32]. As an important subbranch of cooperative control [18,34], the topic of formation control [6,21,22,24,25,33,39] has received massive amount of attention due to its close connection with practical applications such as multi-quadcopter systems [3] and multi-rover systems [30,36].

While completing different tasks, a cluster of agents can be affected by factors like system uncertainties and external disturbances [23,35,38] that influence their performance negatively. Under the subject of adaptive control, disturbance observers [7,37] and neural networks (NNs) [5,31] are usually employed for uncertainty estimation to ensure the robustness of the system. In most published results, the implemented NNs are usually two-layer networks like Chebyshev NNs [5], fuzzy wavelet NNs [29] and radial basis function NNs [40].

Although two-layer networks are famous for their simplicity, three-layer NNs are trusted more for the approximation of unknown functions with strong nonlinearities. In [19], the dynamic programming approach

was used along with a three-layer NN to achieve optimised reference tracking. To estimate the uncertain nonlinearities and external disturbances in each individual agent, three-layer NNs were tuned based on the formation tracking error to perform formation control for a group of autonomous underwater vehicles [4].

However, the cooperative weight tuning law in [4] is not fully error-related, leading to the potential divergence of weight values. Hence, how to obtain a fully local-error-related cooperative tuning law has become a considerable challenge for multi-agent scenarios.

In the area of control engineering, it is also vital to consider the actuator saturation phenomenon when justifying the applicability of one control scheme. Currently, a convenient way to deal with the saturation effect is to treat it as a bounded disturbance and make corresponding compensation while designing the controller [9,28]. The three-layer NN was first used in [9] to approximate the effect of saturation phenomenon. However, the network weight in the hidden layer is set to be constant in [9], which leads to a lack of adaptiveness. The estimation accuracy is further improved in [28] by constructing adaptive tuning law for the weight matrix in the hidden layer.

Although the tracking-error-based weight tuning approach in [28] is proved to be effective for both saturated and unsaturated systems, the convergence time of the neural estimation error will increase along with the system's initial tracking error.

Furthermore, the neural estimation error will not settle before the tracking error converges. Such features expose the drawbacks of employing variables related to the reference tracking error as the weight tuning criterion in systems with actuator saturation. Therefore, it is necessary to develop a finite-time tuning approach that adjusts the neural weights regardless of the reference tracking error.

To ensure that the amplitude of the control input is restricted within the saturation limitation, many researchers choose to implement smooth and bounded functions within the controller design [12,15,20]. Currently, plenty of results have been obtained for systems without input coupling effect [1,12]. An adaptive reaching-law-based sliding mode control approach was developed for formation tracking of electromagnetic systems in [12] to achieve finite-time and chattering-free error convergence. In [1], one compensation term was introduced along with an auxiliary system for a class of discrete-time system to perform adaptive control based on reinforcement learning .

Similarly, saturated functions are also applied in the controller design of coupled systems. For example, a saturation function was added into the controller in [8] to deal with the input saturation problem for a cluster of marine surface vehicles. Additional control terms were introduced in [15] to deal with the input saturation issue of underwater vehicles.

However, obvious oscillations of system states were observed in [8], while chattering phenomenons were recorded for control inputs in [15]. Such observations indicate that the amplitude limitation of control input is not the only concern for systems that have both coupled and saturated actuators. Hence, it is essential to investigate the joint effect of actuator saturation and input coupling effect.

Motivated by the aforementioned gaps and challenges, this paper focuses on the formation control problem for a group of uncertain first-order agents with coupled and saturated actuators. The contributions of this article are:

1. In contrast to the partially error-related weight tuning laws in [4,31], this study proposes a fully local-error-related cooperative weight tuning method for three-layer NN-based function approximators to avoid the divergence of approximation error and further construct an adaptive formation control scheme for multi-agent systems.
2. To reduce the convergence time of the error states within the neural-based observer structure proposed in [19], a fractional-order term is employed to ensure that the observation error is bounded within finite time regardless of the reference tracking errors.
3. Motivated by [8], this paper derives a framework for investigating the joint effect of input coupling and actuator saturation, and further defines the correlated issue as the reverse effect. A new algorithm is also proposed to attenuate the oscillation in error-related states caused by the reverse effect.

Notation: In this paper, let $\|\mathcal{M}\|_F$ denote the Frobenius norm of matrix $\mathcal{M}$. If $\mathcal{M}$ is a square matrix, let $\overline{\sigma}(\mathcal{M})$ and $\underline{\sigma}(\mathcal{M})$ denote the maximum eigenvalue and the minimum eigenvalue of $\mathcal{M}$, respectively. R^+ denotes the set of positive real numbers. $\otimes$ represents the Kronecker production. I_n stands for an n-dimensional identity matrix throughout this paper.

2 Preliminaries

2.1 System model

Consider a distributed nonlinear multi-agent system consists of N first-order agents, and the dynamics of the ith agent is given as

$$\dot{x}_i = f_i(x_i) + g_i(x_i, \mathbf{P}_i)\mathcal{S}_i(u_i) + \bar{w}_i,\ i = 1, 2, \ldots, N \tag{1}$$

where $x_i \in \mathbb{R}^n$ is the position information of the ith agent, $g_i(x_i, \mathbf{P}_i) \in \mathbb{R}^{n\times n}$ is the nonlinear control gain matrix, $\mathbf{P}_i$ represents the model parameter set, $u_i \in \mathbb{R}^n$ is the control input, $f_i(x_i) \in \mathbb{R}^n$ is the unknown dynamics of the system, $\bar{w}_i \in \mathbb{R}^n$ represents the external disturbance, $\mathcal{S}_i(\cdot)$ is the actuator saturation phenomenon and $\mathcal{S}_i(u_i) \in \mathbb{R}^n$ is the saturated control input. The jth element of $\mathcal{S}_i(u_i)$ is expressed as

$$\mathcal{S}_i(u_i(j)) = \begin{cases} u_i(j) & |u_i(j)| \le U_{Mi} \\ \text{sign}(u_i(j))U_{Mi} & |u_i(j)| > U_{Mi} \end{cases} \tag{2}$$

where $u_i(j)$ is the jth element of u_i and $U_{Mi} \in \mathbb{R}^+$ is the saturation limit. Obtaining the value of $g_i(x_i, \mathbf{P}_i)$ is necessary for controller design, but it is hard to obtain the precise value of $\mathbf{P}_i$ with the existence of measurement error. If define $\widehat{\mathbf{P}}_i$ to be our measurement of the parameter set, then the control gain matrix we obtain through calculation is $\widehat{g}_i(x_i, \widehat{\mathbf{P}}_i) \in \mathbb{R}^{n\times n}$, and the parameter estimation error is given as $\widetilde{\mathbf{P}}_i = \mathbf{P}_i - \widehat{\mathbf{P}}_i$. Define $\widetilde{g}_i(x_i, \widetilde{\mathbf{P}}_i) = g_i(x_i, \mathbf{P}_i) - \widehat{g}_i(x_i, \widehat{\mathbf{P}}_i)$ to represent the modelling error of the input coupling matrix, we then have:

$$\dot{x}_i = \widehat{g}_i(x_i, \widehat{\mathbf{P}}_i)\mathcal{S}_i(u_i) + E_i \tag{3}$$

where $E_i = \widetilde{g}_i(x_i, \widetilde{\mathbf{P}}_i)\mathcal{S}_i(u_i) + \bar{w}_i + f_i(x_i)$ represents the combination of unknown factors. For simplicity, we will use g_i and $\widehat{g}_i$ to represent $g_i(x_i, \mathbf{P}_i)$ and $\widehat{g}_i(x_i, \widehat{\mathbf{P}}_i)$, respectively, unless specially stated.

Then we have the dynamics of the cluster as follows:

$$\dot{x} = \widehat{g}\mathcal{S}(u) + E \tag{4}$$

where

$$\begin{aligned} x &= [x_1^{\mathrm{T}}, x_2^{\mathrm{T}}, \ldots, x_N^{\mathrm{T}}]^{\mathrm{T}} \in \mathbb{R}^{nN} \\ \widehat{g} &= \text{diag}\{\widehat{g}_1, \widehat{g}_2, \ldots, \widehat{g}_N\} \in \mathbb{R}^{nN\times nN} \\ \mathcal{S}(u) &= [\mathcal{S}_1^{\mathrm{T}}(u_1), \mathcal{S}_2^{\mathrm{T}}(u_2), \ldots, \mathcal{S}_N^{\mathrm{T}}(u_N)]^{\mathrm{T}} \in \mathbb{R}^{nN} \\ E &= [E_1^{\mathrm{T}}, E_2^{\mathrm{T}}, \ldots, E_N^{\mathrm{T}}]^{\mathrm{T}} \in \mathbb{R}^{nN} \end{aligned}$$

Definition 1 [10] Consider a vector X, we have a correlated continuous Lyapunov function $V(X)$. Then the vector X is said to be semi-globally uniformly ultimately bounded (SGUUB) if $V(X)$ satisfies $V(X) = 0$ only when $\|X\| = 0$, and there exists a positive boundary b_X and a time $t_X(X(t_0), b_X)$ such that $\|V(X)\| \le b_X$ for all $t \ge t_X + t_0$ and $X(t_0) \in \Omega_X^V$, where t_0 is the initial time, $X(t_0)$ is the initial value of X and Ω_X^V is a compact set of X.

Lemma 1 [10] *Consider a vector X that satisfies $X(t_0) \in \Omega_X^V$ and its correlated continuous Lyapunov function $V(X)$, if we have $\dot{V}(X) < 0$ when $\|X\| > b_X$, then $\|X\|$ is said to be SGUUB within the neighbourhood of* $[0, b_X]$.

The position and velocity references of the ith agent are described by $x_{di} \in \mathbb{R}^n$ and $\dot{x}_{di} \in \mathbb{R}^n$, respectively. The main purpose of the controller design is to ensure the semi-global uniform ultimate boundedness of each uncertain agent's reference tracking error with the actuator saturation (2), which is illustrated as

$$\begin{aligned} &\lim_{t\to\infty} \|x_i(t) - x_{di}(t)\| \le \rho,\ \forall x_i(t_0) \in \Omega_x, \\ &\quad i = 1, 2, \ldots, N \end{aligned} \tag{5}$$

where Ω_x is a compact set of x_i and ρ is a small and positive constant.

Assumption 1 The state references x_{di} and $\dot{x}_{di}$ are known and bounded when $t \ge t_0$. The parameter measurement error $\widetilde{\mathbf{P}}_i$ is also bounded.

Assumption 2 There is a known positive constant τ_i and a finite time t_s for the ith agent such that the following inequality is satisfied when $t \ge t_s$

$$|g_i^{-1}(t)(\dot{x}_{di}(t) - f_i(x_i(t)) - \bar{w}_i(t))| \le \tau_i \mathbf{1}_{n\times 1}$$

where $\tau_i < U_{Mi}$ and $\mathbf{1}_{n\times 1}$ is an n-dimensional column vector whose every entry is 1.

Remark 1 Notice that Assumption 2 is made to ensure that the formation tracking process is feasible to the saturated agents in (1) after a finite amount of time. In an ideal situation where $u_i = g_i^{-1}(t)(\dot{x}_{di}(t) - f_i(x_i(t)) - \bar{w}_i(t))$, we can have $\dot{x}_i = \dot{x}_{di}$, meaning that the agent can successfully track the velocity reference. However, it is still necessary to have a residual amount of control input to reduce the value of $\|x_i(t) - x_{di}(t)\|$ when $\|x_i(t_0) - x_{di}(t_0)\| > \rho$, where $x_i(t_0)$ and $x_{di}(t_0)$ are the initial system state and the initial position reference.

Hence, we have $\tau_i < U_{Mi}$ to offer the redundancy in the control input. The time t_s is defined to mark the time when the formation tracking task is feasible to each agent in (4).

2.2 Graph theory

In this paper, the communication topology of the distributed multi-agent system is illustrated by a directed graph $G = \{\mathcal{R}, \mathcal{E}, \mathcal{A}\}$, where $\mathcal{R} = \{r_1, r_2, \ldots, r_N\}$ represents the set of nodes, $\mathcal{E} \subseteq R \times R$ stands for the set of edges and $\mathcal{A} = [a_{ij}] \in \mathbb{R}^{N\times N}$ is the adjacency matrix with nonnegative entries. An edge of the graph G is illustrated as $e_{ij} = (r_i, r_j)$, which stands for an edge points from node r_i to node r_j. Self-loops are not considered in this paper and $a_{ji} = 1$ if and only if $e_{ij} \in E$. We define $\deg_{\text{in}}(r_i) = \sum_{j=1}^{N} a_{ij}$ to be the in-degree of the ith node and the degree matrix of the graph is illustrated as $\mathcal{D} = \text{diag}\{\deg_{\text{in}}(r_i), i = 1, 2, \ldots, N\}$. The Laplacian matrix of the graph is defined as $L = \mathcal{D} - \mathcal{A}$ [14]. If there always exists a directed path between a pair of distinguished nodes, then the directed graph G is said to be strongly connected. In this paper, the communication topology of the multi-agent system (4) is chosen as a strongly connected directed graph. The following lemma is useful for the stability analysis of the proposed control scheme.

Lemma 2 [14] *Define $B \in \mathbb{R}^{n\times n}$ to be a nonnegative diagonal matrix with at least one positive element. If the graph G is strongly connected, then its corresponding Laplacian matrix L satisfies that the matrix $(L + B)$ is an irreducible nonsingular M-matrix. Define*

$$q = [q_1\ q_2\ \ldots\ q_N]^{\mathrm{T}} = (L + B)^{-1} 1_{N\times 1}$$

then we obtain that $P = \text{diag}\{p_i\} = \text{diag}\{1/q_i\}$ is a positive definite matrix. If we define $Q = P(L + B) + (L+B)^{\mathrm{T}} P$, then the matrix Q is symmetric and positive definite.

2.3 Three-layer NN approximation

In this paper, three-layer NNs are implemented to approximate the unknown nonlinear function E_i and act as a part of the adaptive control law. According to the work in [19], an m ($m \geq 3$) layered NN is able to estimate any unknown function with high precision if the input vector of the NN is restricted to its compact set. Define Ω_u to be a compact set of u_i, then the three-layer NN estimation of E_i is written as

$$E_i = W_i^{\mathrm{T}} \mathcal{T}(J_i^{\mathrm{T}} y_i) + \epsilon_i,\ \forall x_i \in \Omega_x,\ u_i \in \Omega_u,\quad i = 1, 2, \ldots, n$$

where $J_i \in \mathbb{R}^{2n\times\bar{n}}$ and $W_i \in \mathbb{R}^{\bar{n}\times n}$ are the optimal weight matrices, $y_i = [x_i^{\mathrm{T}}, u_i^{\mathrm{T}}]^{\mathrm{T}} \in \mathbb{R}^{2n}$ is the input vector of the NN, $\bar{n} \in \mathbb{R}$ is the number of neurons in the hidden layer, $\epsilon_i \in \mathbb{R}^n$ is the network bias and $\mathcal{T}(\cdot)$ is the hyperbolic tangent activation function of the hidden layer. Define $\bar{y}_j$ as the jth element of the vector $J_i^{\mathrm{T}} y_i$, then the jth element of $\mathcal{T}(J_i^{\mathrm{T}} y_i)$ has the following expression:

$$\mathcal{T}(\bar{y}_j) = \frac{e^{\bar{y}_j} - e^{-\bar{y}_j}}{e^{\bar{y}_j} + e^{-\bar{y}_j}}$$

The estimation process of a three-layer NN is

$$\widehat{E}_i = \widehat{W}_i^{\mathrm{T}} \mathcal{T}(\widehat{J}_i^{\mathrm{T}} y_i) \tag{6}$$

where $\widehat{J}_i$ and $\widehat{W}_i$ are the estimated weight matrices.

The estimation error of the NN is given as

$$\widetilde{E}_i = E_i - \widehat{E}_i = \widetilde{W}_i^{\mathrm{T}} \mathcal{T}(\widehat{J}_i^{\mathrm{T}} y_i) + \bar{\epsilon}_i(y_i)$$

where $\bar{\epsilon}_i(y_i) = W_i^{\mathrm{T}}[\mathcal{T}(J_i^{\mathrm{T}} y_i) - \mathcal{T}(\widehat{J}_i^{\mathrm{T}} y_i)] + \epsilon_i$ and $\widetilde{W}_i = W_i - \widehat{W}_i$.

Assumption 3 The approximation compact set Ω_u includes the neighbourhood of $[-U_{Mi}, U_{Mi}]$ for each individual agent.

Assumption 4 The weight matrices W, J and the estimation error ϵ are bounded such that there are positive constants W_M, J_M and ϵ_M that satisfy

$$\|W\|_F \leq W_M,\ \|J\|_F \leq J_M,\ \|\epsilon\| \leq \epsilon_M$$

where we have

$$\epsilon = [\epsilon_1^{\mathrm{T}}, \epsilon_2^{\mathrm{T}}, \ldots, \epsilon_N^{\mathrm{T}}]^{\mathrm{T}} \in \mathbb{R}^{nN}$$
$$W = \text{diag}\{W_1, W_2, \ldots, W_N\} \in \mathbb{R}^{\bar{n}N\times nN}$$
$$J = \text{diag}\{J_1, J_2, \ldots, J_N\} \in \mathbb{R}^{2nN\times\bar{n}N}$$

Lemma 3 [19] *Based on the boundedness of the activation function $\mathcal{T}(\cdot)$, the NN approximation error ϵ and the optimal weight matrices W and J, there exist positive constants $\mathcal{T}_{Mi}$, $\bar{\epsilon}_{Mi}$, $\mathcal{T}_M$ and $\bar{\epsilon}_M$ such that:*

$$\|\mathcal{T}(\widehat{J}_i^{\mathrm{T}} y_i)\| \leq \mathcal{T}_{Mi},\quad \|\bar{\epsilon}_i(y_i)\| \leq \bar{\epsilon}_{Mi}$$
$$\|\mathcal{T}(\widehat{J}^{\mathrm{T}} y)\| \leq \mathcal{T}_M,\quad \|\bar{\epsilon}(y)\| \leq \bar{\epsilon}_M$$

where $\bar{\epsilon}(y) = [\bar{\epsilon}_1^{\mathrm{T}}(y_1), \bar{\epsilon}_2^{\mathrm{T}}(y_2), \ldots, \bar{\epsilon}_N^{\mathrm{T}}(y_N)]^{\mathrm{T}}$.

3 Main results

3.1 Neural-based formation control for unsaturated multi-agent systems

In this subsection, the saturation phenomenon is removed by setting $U_{Mi} = +\infty$. According to the agent dynamics (3), we have

$$\delta_{xi} = x_i - x_{di} \tag{7}$$

where $\delta_{xi} \in \mathbb{R}^n$ is the position tracking error of the ith agent.

Then we have the global form as follows:

$$\delta_x = x - x_d \tag{8}$$

where

$$\delta_x = [\delta_{x1}^{\mathrm{T}}, \delta_{x2}^{\mathrm{T}}, \ldots, \delta_{xN}^{\mathrm{T}}]^{\mathrm{T}} \in \mathbb{R}^{nN}$$
$$x_d = [x_{d1}^{\mathrm{T}}, x_{d2}^{\mathrm{T}}, \ldots, x_{dN}^{\mathrm{T}}]^{\mathrm{T}} \in \mathbb{R}^{nN}$$

Define $b_i \in \mathbb{R}^+$ to be the ith diagonal element of B, the local formation tracking error of the ith agent is obtained as

$$e_{xi} = \sum_{j=1}^{N} a_{ij}(\delta_{xi} - \delta_{xj}) + b_i\delta_{xi} = \sum_{j=1}^{N} l_{ij}\delta_{xj} + b_i\delta_{xi} \tag{9}$$

where l_{ij} is the element on the ith row and jth column of L. In (9), the practical meaning of b_i is the ith agent's sensitivity on its own reference tracking error δ_{xi}. Define $e_x = [e_{x1}^{\mathrm{T}}, e_{x2}^{\mathrm{T}}, \ldots, e_{xN}^{\mathrm{T}}]^{\mathrm{T}}$, we then have the following global form:

$$e_x = (L + B) \otimes I_n\delta_x \tag{10}$$

The time derivative of (10) is obtained as

$$\dot{e}_x = (L + B) \otimes I_n(\widehat{g}u + E - \dot{x}_d) \tag{11}$$

To perform adaptive estimation, the weight tuning law set of a three-layer NN is usually chosen as [4,31]:

$$\dot{\widehat{W}}_i = \Gamma_1 G_W(e_{xi}, \widehat{J}_i, \widehat{W}_i, y_i) - \Gamma_2\widehat{W}_i$$
$$\dot{\widehat{J}}_i = \Gamma_3 G_J(e_{xi}, \widehat{J}_i, \widehat{W}_i, y_i) - \Gamma_4\widehat{J}_i$$

where $\Gamma_i \in \mathbb{R}^+ (i \in [1, 4])$ are the error-invariant tuning gains, and G_W and G_J represent the related tuning functions that satisfy $\|G_W\|_F = \|G_J\|_F = 0$ when $\|e_{xi}\| = 0$ (G_W and G_J will no longer affect W_i when there is no error).

In [4], parameters Γ_2 and Γ_4 are set to be static. Although it is reasonable to include terms like $-\Gamma_2\widehat{W}_i$ and $-\Gamma_4\widehat{J}_i$ to attenuate the oscillation of neural weights when the value of $\|e_{xi}\|$ is high, such terms will also lead to contradictions that $\dot{\widehat{W}}_i = -\Gamma_2\widehat{W}_i$ and $\dot{\widehat{J}}_i = -\Gamma_4\widehat{J}_i$ when $\|e_{xi}\| = 0$, meaning that a potential divergence of estimation error always exists unless $\|W_i\|_F = \|J_i\|_F = 0$ or $\Gamma_2 = \Gamma_4 = 0$.

To deal with the estimation error divergence issue, the idea of selecting Γ_2 and Γ_4 as time-related exponentially decreasing functions is proposed in [31]. Although such approach is found to be effective, it does introduce the danger that the NN will lose the protection of $-\Gamma_2\widehat{W}_i$ and $-\Gamma_4\widehat{J}_i$ after certain period of time, leading to potential chattering or oscillation.

To maintain the protection of $-\Gamma_2\widehat{W}_i$ and $-\Gamma_4\widehat{J}_i$ while avoiding the divergence issue, a fully error-related tuning approach was then proposed in [19]. However, this approach is never investigated in a cooperative way for multi-agent systems. Therefore, we propose a set of fully local-error-related tuning laws of $\widehat{W}_i$ and $\widehat{J}_i$ as the following equations, respectively:

$$\dot{\widehat{W}}_i = \eta_1\mathcal{T}(\widehat{J}_i^{\mathrm{T}}y_i)e_{xi}^{\mathrm{T}} - \eta_2\|e_{xi}\|\widehat{W}_i$$
$$\dot{\widehat{J}}_i = \frac{\eta_3}{2nN}\mathrm{sign}(y_i)e_{xi}^{\mathrm{T}}\widehat{W}_i^{\mathrm{T}}(I_{\bar{n}} - \alpha(\widehat{J}_i^{\mathrm{T}}y_i)) - \eta_4\|e_{xi}\|\widehat{J}_i \tag{12}$$

where $\alpha(\widehat{J}_i^{\mathrm{T}}y_i) = \mathrm{diag}\{\mathcal{T}_j^2(\widehat{J}_i^{\mathrm{T}}y_i)\}$, $j \in [1, \bar{n}]$ and $\eta_i \in \mathbb{R}^+$ $(i = 1, 2, 3, 4)$. Then we have $\|\dot{\widehat{W}}_i\|_F = \|\dot{\widehat{J}}_i\|_F = 0$ when $\|e_{xi}\| = 0$, while $-\eta_2\|e_{xi}\|\widehat{W}_i$ and $-\eta_4\|e_{xi}\|\widehat{J}_i$ remain to be the counter parts to reduce the chattering in the network output without triggering the divergence of the NN estimation error. Accordingly, we have the global form as

$$\dot{\widehat{W}} = \eta_1\mathcal{T}(\widehat{J}^{\mathrm{T}}y)e_x^{\mathrm{T}} - \eta_2\Delta_e \otimes I_{\bar{n}}\widehat{W}$$
$$\dot{\widehat{J}} = \frac{\eta_3}{2nN}\mathrm{sign}(y)e_x^{\mathrm{T}}\widehat{W}^{\mathrm{T}}(I_{\bar{n}N} - \alpha(\widehat{J}^{\mathrm{T}}y)) - \eta_4\Delta_e \otimes I_{2n}\widehat{J} \tag{13}$$

where the following equations are applied:

$$\widehat{W} = \mathrm{diag}\{\widehat{W}_1, \widehat{W}_2, \ldots, \widehat{W}_N\} \in \mathbb{R}^{\bar{n}N \times nN}$$
$$\widehat{J} = \mathrm{diag}\{\widehat{J}_1, \widehat{J}_2, \ldots, \widehat{J}_N\} \in \mathbb{R}^{2nN \times \bar{n}N}$$
$$\Delta_e = \mathrm{diag}\{\|e_{x1}\|, \|e_{x2}\|, \ldots, \|e_{xN}\|\} \in \mathbb{R}^{N \times N}$$
$$y = \left[y_1^{\mathrm{T}}, y_2^{\mathrm{T}}, \ldots, y_N^{\mathrm{T}}\right]^{\mathrm{T}} \in \mathbb{R}^{2nN \times 1}$$

Based on the NN estimation (6) and the weight tuning law set (13), the cooperative formation controller is designed as

$$u_i = \widehat{g}_i^{-1}(\dot{x}_{di} - \widehat{E}_i - k_i e_{xi}) \tag{14}$$

Now we are ready to present the first main result in this paper.

Theorem 1 *Consider system (4) without actuator saturation ($U_{Mi} = +\infty$), and Assumptions 1 and 4 hold. By the three-layer NN estimation (6), the weight tuning law set (12), and the formation controller (14), the system states e_x, δ_x, $\widetilde{W}$ and $\widetilde{J}$ are SGUUB if the following conditions are met:*

1. *The parameters η_2, η_3 and η_4 in (12) and (13) satisfy $\eta_2 > \eta_3/2$ and $\eta_4 > \eta_3/2$.*
2. *The compact set conditions of the NN hold such that we have $x_i(t) \in \Omega_x$ and $u_i(t) \in \Omega_u$ when $t \geq t_0$.*

Proof If we define $\widetilde{W} = W - \widehat{W}$ and $\widetilde{J} = J - \widehat{J}$, we construct the following Lyapunov function candidate:

$$V_1 = \frac{1}{2} e_x^{\mathrm{T}} \mathcal{P} e_x + \frac{1}{2}\mathrm{tr}\{\widetilde{W}^{\mathrm{T}}\widetilde{W}\} + \frac{1}{2}\mathrm{tr}\{\widetilde{J}^{\mathrm{T}}\widetilde{J}\} \tag{15}$$

where $\mathcal{P} = P \otimes I_n$. By Lemma 2, we have

$$\begin{aligned}
\dot{V}_1 &= e_x^{\mathrm{T}}\mathcal{P}[(L+B)\otimes I_n]\dot{\delta}_x - \mathrm{tr}\{\widetilde{W}^{\mathrm{T}}\dot{\widehat{W}}\} - \mathrm{tr}\{\widetilde{J}^{\mathrm{T}}\dot{\widehat{J}}\} \\
&= \frac{1}{2} e_x^{\mathrm{T}}\mathcal{Q}\bar{\epsilon} - \frac{1}{2} e_x^{\mathrm{T}}\mathcal{Q}K e_x + \eta_4 \mathrm{tr}\{\widetilde{J}^{\mathrm{T}}\Delta_e \otimes I_{2n}(J - \widetilde{J})\} \\
&\quad - \mathrm{tr}\left\{\widetilde{J}^{\mathrm{T}}\frac{\eta_3}{2nN}\mathrm{sign}(y) e_x^{\mathrm{T}}\widehat{W}^{\mathrm{T}}(I_{N\bar{n}} - \alpha(\widehat{J}^{\mathrm{T}}y))\right\} \\
&\quad + \mathrm{tr}\left\{\widetilde{W}^{\mathrm{T}}\mathcal{T}(\widehat{J}^{\mathrm{T}}y) e_x^{\mathrm{T}}\left(\frac{1}{2}\mathcal{Q} - \eta_1 \otimes I_{nN}\right)\right\} \\
&\quad + \eta_2 \mathrm{tr}\{\widetilde{W}^{\mathrm{T}}\Delta_e \otimes I_{\bar{n}}(W - \widetilde{W})\}
\end{aligned}$$

where we have $K = \mathrm{diag}\{k_1, k_2, \ldots, k_N\} \otimes I_n$ and $\mathcal{Q} = (P(L+B)) \otimes I_n$. With the following inequalities:

$$\begin{aligned}
&\mathrm{tr}\{\widetilde{W}^{\mathrm{T}}(W - \widetilde{W})\} \leq W_M \|\widetilde{W}\|_F - \|\widetilde{W}\|_F^2 \\
&\mathrm{tr}\{\widetilde{J}^{\mathrm{T}}(J - \widetilde{J})\} \leq J_M \|\widetilde{J}\|_F - \|\widetilde{J}\|_F^2 \\
&\Delta_e \leq \|e_x\| \otimes I_N, \quad \left\|\frac{1}{2nN}\mathrm{sign}(y)\right\| \leq 1
\end{aligned}$$

we further obtain that

$$\begin{aligned}
\dot{V}_1 \leq &-\frac{1}{2}\underline{\sigma}(\mathcal{Q}K)\|e_x\|^2 + (r_1\|\widetilde{W}\|_F + r_2 - \eta_2\|\widetilde{W}\|_F^2 \\
&+ r_3\|\widetilde{J}\|_F + \eta_3\|\widetilde{W}\|_F\|\widetilde{J}\|_F - \eta_4\|\widetilde{J}\|_F^2)\|e_x\|
\end{aligned} \tag{16}$$

where we have $r_1 = \overline{\sigma}(\mathcal{Q}/2 - \eta_1 \otimes I_{nN})\mathcal{T}_M + \eta_2 W_M$, $r_2 = \overline{\sigma}(\mathcal{Q})\bar{\epsilon}_M/2$ and $r_3 = \eta_3 W_M + \eta_4 J_M$.

With the parameters chosen as $\eta_2 > \eta_3/2$ and $\eta_4 > \eta_3/2$, we can rewrite (16) into the following form:

$$\dot{V}_1 \leq -\frac{1}{2}\underline{\sigma}(\mathcal{Q}K)\|e_x\|^2 + r_4\|e_x\| \tag{17}$$

where $r_4 = r_3^2/(4\eta_4 - 2\eta_3) + r_1^2/(4\eta_2 - 2\eta_3) + r_2$. Hence, $\dot{V}_1$ will remain negative when e_x belongs to the following region:

$$\Omega_e = \left\{ e_x \middle| \|e_x\| > \frac{2r_4}{\underline{\sigma}(\mathcal{Q}K)} \right\} \tag{18}$$

By (10), we also have that the reference tracking error is SGUUB within the following neighbourhood:

$$\Omega_\delta = \left\{ \delta_x \middle| \|\delta_x\| \leq \frac{2r_4}{\underline{\sigma}(\mathcal{Q}K)\underline{\sigma}(L+B)} \right\}$$

By the Lyapunov theory extension in [13], both $\widetilde{W}$ and $\widetilde{J}$ are SGUUB, which completes the proof. □

Although the cooperative tuning approach (12) can guarantee the semi-global uniform ultimate boundedness of the error states e_x and δ_x, its performance is questionable when there exists the actuator saturation phenomenon (2).

Theoretically, the error-related weight tuning procedure (12) will not settle before $\|e_{xi}\|$ converges to a neighbourhood around 0. Correspondingly, the settling time for the weight tuning process is expected to be prolonged along with the increment in each agent's initial local formation tracking error because of the actuator saturation in (2). Hence, further investigation is essential to explore a more suitable way to implement three-layer NNs when the system is saturated.

3.2 Observer-based formation control for uncertain and saturated multi-agent systems

Now we consider the systems with saturated actuators. In most of the previous research works like [8,12], the only issue regarding saturation is considered as restricting the amplitude of each element in the control input within the saturation limitation U_{Mi}. However, such results are far from sufficient for a system that has coupled and saturated control inputs like (3).

For example, consider a two-dimensional first-order system that has two control inputs that are coupled and suppose that the calculated nominal control input is obtained as the two dotted vectors U_1 and U_2 as shown

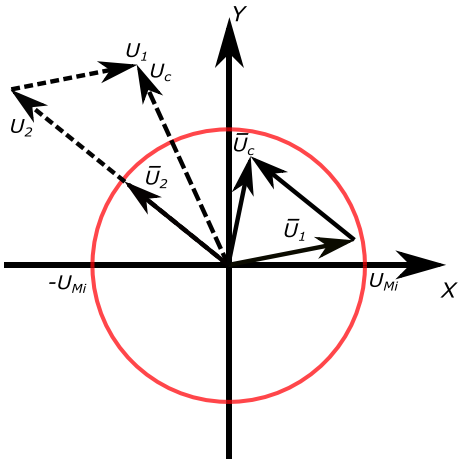

Fig. 1 Saturation's effect on coupled control input

in Fig. 1, where the circle with the radius of U_{Mi} represents the saturation limitation.

If the saturation phenomenon is ruled out, we can then obtain the dotted vector U_c as the combined control input, which is expected to bring about a negative speed in the X direction. However, the amplitude of U_2 will be reduced to $\bar{U}_2$ if the controller is saturated (as the solid vector shows), which will further lead to a saturated combined control input $\bar{U}_c$ that imposes an opposite result in the X direction. Such circumstances will lead to elevations or fluctuations of the system's formation tracking error. To have further investigation, we first define the aforementioned behaviour as the reverse effect of coupled actuator saturation phenomenons.

Definition 2 For a saturated system whose control input is coupled and saturated like (3), the control input is said to be affected by the reverse effect of coupled actuator saturation if the following equation stands:

$$\text{sign}(g_i u_i) \neq \text{sign}(g_i \mathcal{S}_i(u_i))$$

Moreover, as we mentioned in Sect. 3.1, the saturation phenomenon will also delay the cooperative neural tuning procedure (12) because the output of the NN cannot be fully reflected by the control input due to the saturation phenomenon. It is unreasonable to employ a weight tuning process (12) that cannot guarantee the semi-global uniform ultimate boundedness of $\widetilde{W}$ and $\widetilde{J}$ before the convergence of e_x and δ_x. As a result, apart from the aim to make the control input bounded, two more problems correlated with the saturation phenomenon are worthy of further discussion:

Problem 1 How to have a finite-time NN-based estimation of system uncertainties regardless of the reference tracking errors δ_{xi} and e_{xi}?

Problem 2 How to ensure that the coupled controller can provide control inputs with correct combined control direction to attenuate the reverse effect?

Regarding the first problem, we reconstruct the previous three-layer NN into a finite-time observer as follows with the inspiration from [19]:

$$\dot{\widehat{x}}_i = \widehat{g}_i u_i + \widehat{E}_i + \gamma_i \text{diag}\{\text{sign}(\widetilde{x}_i)\}|\widetilde{x}_i|^{\beta_i} \tag{19}$$

where $\widetilde{x}_i = x_i - \widehat{x}_i$, $\gamma_i \in \mathbb{R}^{n\times n}$ is a positive definite constant diagonal matrix and β_i is a real number that satisfies $\beta_i \in (0.5, 1)$.

The weight tuning law set of the NN is chosen as follows:

$$\begin{aligned}\dot{\widehat{W}}_i =& \eta_1 \mathcal{T}(\widehat{J}_i^{\mathrm{T}} y_i)\widetilde{x}_i^{\mathrm{T}} - \eta_2 \|\widetilde{x}_i\| \widehat{W}_i \\ \dot{\widehat{J}}_i =& \frac{\eta_3}{\|\text{sign}(y_i)\|}\text{sign}(y_i)\widetilde{x}_i^{\mathrm{T}}\widehat{W}_i^{\mathrm{T}}(I_{\bar{n}} - \alpha(\widehat{J}_i^{\mathrm{T}} y_i)) \\ & - \eta_4 \|\widetilde{x}_i\| \widehat{J}_i\end{aligned} \tag{20}$$

Then the error dynamics of the neural-based observer is obtained as

$$\dot{\widetilde{x}}_i = \widetilde{E}_i - \gamma_i \text{diag}\{\text{sign}(\widetilde{x}_i)\}|\widetilde{x}_i|^{\beta_i} + \widehat{g}_i(\mathcal{S}_i(u_i) - u_i) \tag{21}$$

The following assumption is made to ensure the boundedness of the initial error in (19):

Assumption 5 The error states $\widetilde{x}_i$, $\widetilde{W}_i$ and $\widetilde{J}_i$ are all bounded such that

$$\begin{aligned}&\widetilde{x}_i^{\mathrm{T}}(t_0)\widetilde{x}_i(t_0) + \text{tr}\{\widetilde{W}_i^{\mathrm{T}}(t_0)\widetilde{W}_i(t_0)\} \\ &\quad + \text{tr}\{\widetilde{J}_i^{\mathrm{T}}(t_0)\widetilde{J}_i(t_0)\} \leq \mathcal{V}_e\end{aligned}$$

where $\mathcal{V}_e$ is a positive constant.

Before we present our result in the observer design, we first recall one useful result:

Lemma 4 [11] *For a continuous Lyapunov function $V(X)$ that satisfies:*

$$\dot{V} \leq -\rho_1 V^{\bar{\rho}}(t) + \rho_2 V^{1/2}(t)$$

the state X is globally finite-time UUB within the region of $\Omega_V = \{X | V(X)^{\bar{\rho}-1/2} < \rho_2/\bar{\rho}_1\}$, where $\bar{\rho}_1 \in (0, \rho_1)$, $\bar{\rho} > 1/2$, $\rho_1, \rho_2 > 0$. The settling time T is bounded by:

$$T \leq \frac{V^{1-\bar{\rho}}(t_0)}{(\rho_1 - \bar{\rho}_1)(1-\bar{\rho})}$$

Then we have the next result on the finite-time observer design.

Theorem 2 *Consider system (3) with actuator saturation (2), where Assumptions 1, 3, 4 and 5 hold. By the neural-based observer (19), and the weight tuning law set (20), the semi-global uniform ultimate boundedness of $\widetilde{x}_i$, $\widetilde{W}_i$ and $\widetilde{J}_i$ is guaranteed if the following conditions are met:*

1. *The control input satisfies $|u_i| \leq U_{Mi}\mathbf{1}_{n\times 1}$.*
2. *The parameters η_2, η_3 and η_4 in (20) satisfy $\eta_2 > \eta_3/2$ and $\eta_4 > \eta_3/2$.*
3. *The compact set conditions of the NN hold such that we have $x_i(t) \in \Omega_x$ and $u_i(t) \in \Omega_u$ when $t \geq t_0$.*

Furthermore, the observation error $\widetilde{x}_i$ is semi-globally finite-time UUB.

Proof Consider a Lyapunov candidate as follows:

$$V_2 = \frac{\eta_1}{2}\widetilde{x}_i^{\mathrm{T}}\widetilde{x}_i + \frac{1}{2}\mathrm{tr}\{\widetilde{W}_i^{\mathrm{T}}\widetilde{W}_i\} + \frac{1}{2}\mathrm{tr}\{\widetilde{J}_i^{\mathrm{T}}\widetilde{J}_i\} \tag{22}$$

With the control input satisfies $|u_i| \leq U_{Mi}\mathbf{1}_{n\times 1}$, we have $\mathcal{S}_i(u_i) = u_i$, which further leads to

$$\begin{aligned}
\dot{V}_2 &= \eta_1\widetilde{x}_i^{\mathrm{T}}\dot{\widetilde{x}}_i + \mathrm{tr}\{\widetilde{W}_i^{\mathrm{T}}\dot{\widetilde{W}}_i\} + \mathrm{tr}\{\widetilde{J}_i^{\mathrm{T}}\dot{\widetilde{J}}_i\} \\
&= -\gamma_i\eta_1\widetilde{x}_i^{\mathrm{T}}\mathrm{diag}\{\mathrm{sign}(\widetilde{x}_i)\}|\widetilde{x}_i|^{\beta_i} + \eta_1\widetilde{x}_i^{\mathrm{T}}(\widetilde{W}_i^{\mathrm{T}}\mathcal{T}(\widehat{J}_i^{\mathrm{T}}y_i) \\
&\quad + \bar{\epsilon}_i(y_i)) - \eta_1\mathrm{tr}\{\widetilde{W}_i^{\mathrm{T}}\mathcal{T}(\widehat{J}_i^{\mathrm{T}}y_i)\widetilde{x}_i^{\mathrm{T}}\} \\
&\quad - \eta_3\mathrm{tr}\left\{\widetilde{J}_i^{\mathrm{T}}\frac{\mathrm{sign}(y_i)}{\|\mathrm{sign}(y_i)\|}\widetilde{x}_i^{\mathrm{T}}\widehat{W}_i^{\mathrm{T}}(I_n - \alpha(\widehat{J}_i^{\mathrm{T}}y_i))\right\} \\
&\quad + \eta_4\mathrm{tr}\{\widetilde{J}_i^{\mathrm{T}}\|\widetilde{x}_i\|\widehat{J}_i\} + \eta_2\mathrm{tr}\{\widetilde{W}_i^{\mathrm{T}}\|\widetilde{x}_i\|\widehat{W}_i\} \\
&\leq -\underline{\sigma}(\gamma_i)\eta_1\|\widetilde{x}_i\|^{1+\beta_i} + \eta_3\|\widetilde{J}_i\|_F\|\widetilde{x}_i\|(W_{Mi} + \|\widetilde{W}_i\|_F) \\
&\quad - \eta_2\|\widetilde{W}_i\|_F^2\|\widetilde{x}_i\| - \eta_4\|\widetilde{J}_i\|_F^2\|\widetilde{x}_i\| + \eta_1\|\widetilde{x}_i\|\bar{\epsilon}_{Mi} \\
&\quad + \eta_4 J_{Mi}\|\widetilde{J}_i\|_F\|\widetilde{x}_i\| + \eta_2 W_{Mi}\|\widetilde{W}_i\|_F\|\widetilde{x}_i\|
\end{aligned}$$

where $\|W_i\| \leq W_{Mi}$ and $\|J_i\| \leq J_{Mi}$ are applied based on Lemma 3.

Similar to the proof of Theorem 1, if we define $r_5 = \eta_2 W_{Mi}$ and $r_6 = \eta_3 W_{Mi} + \eta_4 J_{Mi}$, we obtain

$$\begin{aligned}
\dot{V}_2 \leq -\|\widetilde{x}_i\|\Bigg[&\eta_1(\underline{\sigma}(\gamma_i)\|\widetilde{x}_i\|^{\beta_i} - \bar{\epsilon}_{Mi}) - \frac{r_5^2}{2(2\eta_2 - \eta_3)} \\
&- \frac{r_6^2}{2(2\eta_4 - \eta_3)}\Bigg]
\end{aligned}$$

Then we have the SGUUB region of $\|\widetilde{x}_i\|$ as follows:

$$\begin{aligned}
\|\widetilde{x}_i\| \leq \Bigg[&\frac{1}{2\eta_1\underline{\sigma}(\gamma_i)}\Bigg(\frac{r_5^2}{(2\eta_2 - \eta_3)} + \frac{r_6^2}{(2\eta_4 - \eta_3)} \\
&+ 2\eta_1\bar{\epsilon}_{Mi}\Bigg)\Bigg]^{1/\beta_i}
\end{aligned} \tag{23}$$

By the Lyapunov theory extension in [13], both $\widetilde{W}$ and $\widetilde{J}$ are also SGUUB. Alternatively, if we select the Lyapunov candidate as follows:

$$V_3 = \frac{1}{2}\widetilde{x}_i^{\mathrm{T}}\widetilde{x}_i$$

We can then obtain the time derivative of V_3 as

$$\begin{aligned}
\dot{V}_3 &= \widetilde{x}_i^{\mathrm{T}}\dot{\widetilde{x}}_i \\
&= -\gamma_i\widetilde{x}_i^{\mathrm{T}}\mathrm{diag}\{\mathrm{sign}(\widetilde{x}_i)\}|\widetilde{x}_i|^{\beta_i} + \widetilde{x}_i^{\mathrm{T}}(\widetilde{W}_i^{\mathrm{T}}\mathcal{T}(\widehat{J}_i^{\mathrm{T}}y_i) \\
&\quad + \bar{\epsilon}_i(y_i)) \\
&\leq -\underline{\sigma}(\gamma_i)\|\widetilde{x}_i\|^{\beta_i+1} + \|\widetilde{x}_i\|\widetilde{w}_M
\end{aligned}$$

where we have that $\widetilde{w}_M$ is a positive constant that satisfies $\|\widetilde{W}_i^{\mathrm{T}}\mathcal{T}(\widehat{J}_i^{\mathrm{T}}y_i) + \bar{\epsilon}_i(y_i)\| \leq \widetilde{w}_M$ due to the boundedness of the NN estimation error.

Define $r_7 = \underline{\sigma}(\gamma_i)\sqrt{2^{\beta_i+1}}$ and $r_8 = \sqrt{2}\widetilde{w}_M$, we have

$$\dot{V}_3 \leq -r_7 V_3^{(\beta_i+1)/2} + r_8 V_3^{1/2} \tag{24}$$

By Lemma 4, $\widetilde{x}_i$ is finite-time UUB. However, because the input of the NN needs to satisfy $x_i \in \Omega_x$ and $u_i \in \Omega_u$, $\widetilde{x}_i$ is considered to be semi-globally finite-time UUB, and the finite-time characteristics of $\|\widetilde{x}_i\|$ remains until it reaches the following neighbourhood:

$$\Omega_{\widetilde{x}} = \left\{\widetilde{x}_i \middle| \|\widetilde{x}_i\| \leq \left(\frac{\widetilde{w}_M}{\underline{\sigma}(\gamma_i)}\right)^{1/\beta_i}\right\} \tag{25}$$

which completes the proof. □

After constructing the finite-time neural-based observer (19), Problem 1 is solved. Next, we consider Problem 2.

To attenuate the previously defined reverse effect of saturation, we first decompose the previous controller design (14) for our analysis:

$$u_i = u_{t,i} + u_{d,i} + u_{e,i} \tag{26}$$

where $u_{t,i} = \widehat{g}_i^{-1}\dot{x}_{di}$ is the control input to maintain the velocity tracking behaviour, $u_{d,i} = -\widehat{g}_i^{-1}\widehat{E}_i$ is the control input to compensate for the estimated system uncertainties, and $u_{e,i} = -k_i\widehat{g}_i^{-1}e_{xi}(k_i \in \mathbb{R}^+)$ is the control input for formation error reduction.

We know that both $u_{t,i}$ and $u_{d,i}$ are consistently needed throughout the formation tracking process. By Assumption 2, we also have

$$\lim_{t\to t_s}|\widehat{g}_i^{-1}(t)(\dot{x}_{di}(t) - \widehat{E}_i)| \leq \tau_i\mathbf{1}_{n\times 1}$$

which indicates that the combination of $u_{t,i}$ and $u_{d,i}$ is bounded after t_s.

By Assumption 5 and Theorem 2, we have a finite time t_o and three positive constants E_M, $\bar{E}_M$ and $\widetilde{E}_M$ that satisfy $|E_i| \leq E_M \mathbf{1}_{n\times 1}$, $|E_i - \widehat{E}_i| \leq \bar{E}_M \mathbf{1}_{n\times 1}$ and $\lim_{t\to t_o} |E_i(t) - \widehat{E}_i(t)| \leq \widetilde{E}_M \mathbf{1}_{n\times 1}$. Based on the boundedness we obtained, we introduce the following smooth projection function [5] $\bar{\mathcal{S}}(\mathcal{V}, \tau_M, \psi_M)$ to improve the performance of our controller:

$$\bar{\mathcal{S}}(\mathcal{V}(j), \tau_M, \psi_M) = \begin{cases} \tau_M + \psi_M(1 - \mathrm{e}^{(\tau_M - \mathcal{V}(j))/\psi_M}), \\ \qquad \text{if } \mathcal{V}(j) > \tau_M \\ \mathcal{V}(j), \qquad \text{if } |\mathcal{V}(j)| \leq \tau_M \\ \psi_M(\mathrm{e}^{(\tau_M + \mathcal{V}(j))/\psi_M} - 1) - \tau_M, \\ \qquad \text{if } \mathcal{V}(j) < -\tau_M \end{cases} \tag{27}$$

where $\mathcal{V}(j)$ denotes the jth element of the column vector $\mathcal{V}$, τ_M is a positive constant, and ψ_M denotes a small positive constant. Then we define $u_{m,i} \in \mathbb{R}^n$ to be the control input to maintain the velocity tracking behaviour for the ith agent:

$$u_{m,i} = \widehat{g}_i^{-1}(\dot{x}_{di} - \bar{\mathcal{S}}(\widehat{E}_i, E_M, \psi_E)) \tag{28}$$

where ψ_E is a small positive constant.

To attenuate the reverse effect of the saturation phenomenon, we propose a control input distribution algorithm (CIDA) that generates a positive variable ξ_i to shrink $u_{e,i}$ as shown in Algorithm 1. The CIDA keeps monitoring if the nominal control input $u^i_{\text{nom}} = u_{m,i} + u_{e,i}$ triggers the reverse effect. If the nominal control input does not exceed the saturation limit, then the controller will run at its maximum effort within the saturation limitation. Otherwise, a series of calculation is performed to generate a shrinking factor $\xi_i \in (0, 1]$ for each agent to reduce the scenarios where $\text{sign}(\widehat{g}_i u_i) \neq \text{sign}(\widehat{g}_i \mathcal{S}_i(u_i))$. Based on the discussions about the neural-based observer (19), the weight tuning law set (20), the formation maintaining control input (28), and Algorithm 1, we have the final design as

$$\bar{u}_i = \bar{\mathcal{S}}(u_{m,i}, \tau_i, \psi_u) + \xi_i u_{e,i} \tag{29}$$

where $\mathcal{S}_i(\bar{u}_i) = \bar{u}_i$ is guaranteed by Algorithm 1.

Based on the results of neural-based observer and the CIDA, we obtain a system design as shown in Fig. 2. Now we are ready to present our new saturated formation controller design:

Theorem 3 *Consider system (4) with actuator saturation (2), and Assumptions 1-5 hold. By the finite-time neural-based observer (19), the weight tuning law set (20), the formation control law (29), and the CIDA (Algorithm 1), the error states e_x and δ_x are SGUUB within the following regions, respectively:*

$$\|e_x\| \leq \frac{\overline{\sigma}(Q)\widetilde{E}_M nN}{\bar{k}\underline{\sigma}(Q)}, \quad \|\delta_x\| \leq \frac{\overline{\sigma}(Q)\widetilde{E}_M nN}{\bar{k}\underline{\sigma}(Q)\underline{\sigma}(L+B)} \tag{30}$$

if the following conditions are met simultaneously:

1. *η_2, η_3 and η_4 in (20) satisfy $\eta_2 > \eta_3/2$ and $\eta_4 > \eta_3/2$*
2. *k_i in (29) satisfies $k_i = \bar{k} > 0 (i = 1, 2, \ldots, N)$*
3. *ψ_u in (29) satisfies $\psi_u < \bar{U}_{Mi} - \widetilde{E}_M - \epsilon_E$*
4. *The compact set conditions of the NN hold such that we have $x_i(t) \in \Omega_x$ and $u_i(t) \in \Omega_u$ when $t \geq t_0$.*

Algorithm 1: Control Input Distribution Algorithm

```
Input: S̄(u_{m,i}, τ_i, ψ_u), u_{e,i}, U_{Mi}
Output: ξ_i
ξ_min = 1 ;
u^i_nom = S̄(u_{m,i}, τ_i, ψ_u) + u_{ei} ;
u^i_sat = S̄(u^i_nom, U_{Mi}, 0) ;
if u^i_nom ≠ u^i_sat then
    u_up = U_{Mi} 1_{n×1} − S̄(u_{m,i}, τ_i, ψ_u) ;
    u_lo = −U_{Mi} 1_{n×1} − S̄(u_{m,i}, τ_i, ψ_u) ;
    for j = 1 : n do
        if u_{e,i}(j) = 0 then
            ξ_i = 1;
        else
            if u_{e,i}(j) > 0 then
                ξ_i = u_up(j)/u_{e,i}(j) ;
            else
                ξ_i = u_lo(j)/u_{e,i}(j) ;
            end
        end
        ξ_min = min(ξ_i, ξ_min) ;
    end
end
ξ_i = ξ_min ;
Return ξ_i ;
```

Proof With the implementation of the shrinking factor ξ_i generated by Algorithm 1, it is hard to use Lyapunov functions to directly obtain a result for the stability analysis. Therefore, we need to first illustrate that the value of ξ_i will converge to 1 within finite time for each individual agent. Then we will use the Lyapunov stability theory to prove that e_x is SGUUB.

The formation tracking procedure of the ith agent is divided into the following three stages:

1. When $t \leq t_f = \max(t_s, t_o)$ and $\xi_i \in [0, 1)$.
2. When $t > t_f = \max(t_s, t_o)$ and $\xi_i \in [0, 1)$.

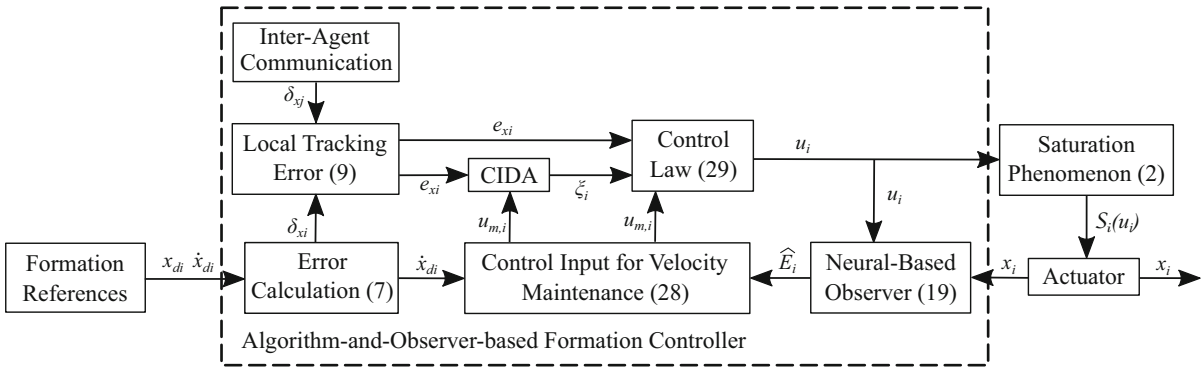

Fig. 2 Robust controller based on CIDA and neural-based observer

3. When $t > t_f = \max(t_s, t_o)$ and $\xi_i = 1$.

To analyse the transformation from one stage to another, we first construct a Lyapunov function regarding the formation tracking error of system (4):

$$V_4 = \frac{1}{2} e_x^{\mathrm{T}} P \otimes I_n e_x$$

Then the time derivative is obtained as

$$\dot{V}_4 = e_x^{\mathrm{T}} P(L+B) \otimes I_n(\widehat{g}\mathcal{S}(\bar{u}) + E - \dot{x}_d)$$

where $\bar{u} = [\bar{u}_1^{\mathrm{T}}, \bar{u}_2^{\mathrm{T}}, \ldots, \bar{u}_N^{\mathrm{T}}]^{\mathrm{T}}$. Based on the knowledge of $\mathcal{S}_i(\bar{u}_i) = \bar{u}_i$, we have

$$\dot{V}_4 = e_x^{\mathrm{T}} P(L+B) \otimes I_n(\widehat{g}\bar{u} + E - \dot{x}_d) \tag{31}$$

For the first stage, we consider one extreme circumstance that equations $\xi_i = 0$ and $|\widetilde{E}_i| = \bar{E}_M \mathbf{1}_{n\times 1}$ remain true until time t_f, when the neural-based observer is settled and the formation tracking task is achievable. With $|\bar{\mathcal{S}}(u_{m,i}, \tau_i, \psi_u)| \le |u_{m,i}|$, we obtain the following equation from (31):

$$\dot{e}_x = (L+B) \otimes I_n(\bar{E}_M \mathbf{1}_{nN\times 1})$$

With $(L \otimes I_n)\bar{E}_M \mathbf{1}_{nN\times 1} = \mathbf{0}_{nN\times 1}$, we have $|\dot{e}_x| \le \overline{\sigma}(B)\bar{E}_M \mathbf{1}_{nN\times 1}$, which further leads to

$$|e_x(t_f)| \le |e_x(t_0)| + t_f \overline{\sigma}(B)\bar{E}_M \mathbf{1}_{nN\times 1}$$

where t_0 is the initial time.

After the finite time t_f, the system (4) is at the second stage, where (31) is expressed as

$$\dot{V}_4 = e_x^{\mathrm{T}} P(L+B) \otimes I_n(\widetilde{E} - \bar{k}\xi \otimes I_n e_x)$$

where

$$\xi = \mathrm{diag}\{\xi_1, \xi_2, \ldots, \xi_N\},\ \widetilde{E} = [\widetilde{E}_1^{\mathrm{T}}, \widetilde{E}_2^{\mathrm{T}}, \ldots, \widetilde{E}_N^{\mathrm{T}}]^{\mathrm{T}}$$

If we define $\bar{U}_{Mi} = U_{Mi} - \tau_i$ to represent the minimum amplitude of the accessible control input for error reduction, it is reasonable to have $\widetilde{E}_M < \bar{U}_{Mi}$ for every agent when $t \ge t_f$.

Define $\underline{e}_x = \min(|e_x|)$ and $\overline{e}_x = \max(|e_x|)$ to represent channels with the lowest and the highest amplitude in vector e_x, respectively. By $\psi_u < \bar{U}_{Mi} - \widetilde{E}_M$, if we define $\widetilde{U}_{Mi} = \bar{U}_{Mi} - \widetilde{E}_M - \psi_u$ to represent the least amount of residual control input for each agent, we are confident to say that the available control input can reduce the amplitude of $\overline{e}_x$ with the speed of

$$\frac{d|\overline{e}_x|}{dt} \le -\underline{\sigma}(L+B)\widetilde{U}_{Mi}$$

For other channels, consider the extreme scenario where $\dot{e}_{xi}(j)e_{xi}(j) > 0$ when $|e_{xi}(j)| < |\overline{e}_x|$. Because the controller parameter k_i is chosen as $k_i = \bar{k}$ for each individual agent, $|e_{xi}(j)|$ will increase until $|e_{xi}(j)| = |\overline{e}_x|$, leading to

$$\begin{cases} \dot{e}_{xi}(j) \le -\underline{\sigma}(L+B)\widetilde{U}_{Mi}, & \text{if } \overline{e}_x > 0 \\ \dot{e}_{xi}(j) \ge \underline{\sigma}(L+B)\widetilde{U}_{Mi}, & \text{if } \overline{e}_x < 0 \end{cases}$$

Thus, the parameter ξ_i is expected to converge to 1 within the finite time of

$$t_\xi = \frac{|\overline{e}_x(t_0)| + t_f\overline{\sigma}(L+B)\bar{E}_M - \widetilde{U}_{Mi}/\bar{k}}{\underline{\sigma}(L+B)\widetilde{U}_{Mi}}$$

Finally, every agent will achieve the third stage after the finite time of $t_f + t_\xi$ to have the following results:

$$\begin{aligned} \dot{V}_4 &= e_x^{\mathrm{T}} P(L+B) \otimes I_n(-\bar{k}e_x + \widetilde{E}) \\ &= -\frac{\bar{k}}{2} e_x^{\mathrm{T}} Q \otimes I_n e_x + \frac{1}{2} e_x^{\mathrm{T}} Q \otimes I_n \widetilde{E} \\ &\le -\frac{\bar{k}}{2}\underline{\sigma}(Q)\|e_x\|^2 + \frac{1}{2}\overline{\sigma}(Q)\|e_x\|\|\widetilde{E}\| \end{aligned} \tag{32}$$

Hence, $\dot{V}_4$ will remain negative unless the following inequalities are satisfied:

$$\|e_x\| \leq \frac{\overline{\sigma}(Q)\widetilde{E}_M nN}{\bar{k}\underline{\sigma}(Q)}, \ \|\delta_x\| \leq \frac{\overline{\sigma}(Q)\widetilde{E}_M nN}{\bar{k}\underline{\sigma}(Q)\underline{\sigma}(L+B)} \tag{33}$$

Note that the neural-based observer (19) only holds semi-global stability. Hence, by Lemma 1, both e_x and δ_x are SGUUB, which completes the proof. □

Remark 2 In (20), parameters η_1 and η_3 both act as the NN's sensitivity to the observation error $\widetilde{x}_i$. Hence, if the values of η_1 and η_3 are increased, the convergence neighbourhood of $\|\widetilde{x}_i\|$ (23) will shrink in theory. However, if we set the values of η_1 and η_3 to be very high, the NN in (6) will be oversensitive to errors, leading to oscillations in its output. On the other hand, both η_2 and η_4 act as the damper to stop the weight matrix from changing rapidly. Hence, increasing the values of η_2 and η_4 will decrease the amount of chattering in the network output, but it will also extend the convergence time of the observation error.

Remark 3 The constant matrix γ_i in (19) acts as the observer's sensitivity to term $\text{diag}\{\text{sign}(\widetilde{x}_i)\}|\widetilde{x}_i|^{\beta_i}$. By both (23) and (25), we see that the convergence region of $\|\widetilde{x}_i\|$ will shrink if we increase the value of $\underline{\sigma}(\gamma_i)$. The effect of β_i is comparatively complex. When $\|\widetilde{x}_i\| \leq 1$, setting β_i close to 0.5 will bring faster convergence speed. However, due to the characteristics of the fractional order, choosing β_i close to 1 will lead to a faster convergence when $|\widetilde{x}_i| > \mathbf{1}_{n\times 1}$.

Remark 4 The purpose of employing the smooth projection law in (28) is to restrict the effect of $\widehat{E}_i$, which will attenuate chattering in the control input u_i and system state x_i if the states in the neural-based observer are experiencing oscillation. Regarding the proportional parameter k_i in term $u_{e,i}$, a rise in its value will result in a decrease in the ultimate convergence region of both δ_x and e_x (see (33)).

Remark 5 The purpose of Assumption 5 is to ensure that the initial estimation error of the neural-based observer is bounded. Related parameters are also useful to prove the finite-time convergence of observation error $\widetilde{x}_i$ and the shrinking factor ξ_i.

4 Simulation

To justify the performance of the proposed neural-based observer (19), the CIDA (Algorithm 1) and the distributed formation control law (29), simulations and comparisons regarding a multi-robot system are provided.

Consider a multi-robot system that contains 6 omni-directional robots [7], and the dynamics of the ith robot is given as

$$\dot{x}_i = T_i(\theta_i, R_i)u_i + \bar{w}_i$$

where $x_i = [p_i^x, p_i^y, \theta_i]^{\mathrm{T}}$ denotes the state vector that contains the position and orientation information of the robot, $u_i = [u_i^1, u_i^2, u_i^3]^{\mathrm{T}}$ represents the speed vector of the robot's motors, $\bar{w}_i$ is the external disturbance vector, and $T_i(\theta_i, R_i)$ is the control gain matrix with the following expression:

$$T_i(\theta_i, R_i) = \begin{bmatrix} -\sin(\theta_i) & -\sin(\pi/3-\theta_i) & \sin(\pi/3+\theta_i) \\ \cos(\theta_i) & -\cos(\pi/3-\theta_i) & -\cos(\pi/3+\theta_i) \\ 1/R_i & 1/R_i & 1/R_i \end{bmatrix}$$

where $R_i \in \mathbb{R}^+$ is the radius of the robot.

With the existence of measurement error, it is hard for us to get the precise value of R_i. Hence, the parameter value that is measured and employed in the controller design process is illustrated as $\widehat{R}_i$. The value of R_i, $\widehat{R}_i$ and the initial state values are provided in Table 1. The actuator saturation limit is set as $U_{Mi} = 0.25$ by Assumption 2.

The communication topology is chosen as Fig. 3 and $b_i = 2$. The system uncertainties and formation references are chosen as follows, respectively:

$$\begin{aligned} \bar{w}_i = [&0.02\cos(0.5t+\pi/2) + 0.03e^{-|p_i^x|-1}, \\ &0.03\sin(0.2t) + 0.02\tanh(p_i^y), \\ &0.04\sin(0.1t+\theta_i) + 0.01\tanh(\theta_i)]^{\mathrm{T}}, \\ x_{di} = [&2\cos(-0.15t+\pi) + 2\cos(i\pi/3) - 1, \\ &2\sin(i\pi/3) + 2\sin(-0.15t+\pi), 0]^{\mathrm{T}}, \\ &i = 1, 2, \ldots, 6 \end{aligned} \tag{34}$$

To justify the effectiveness of our designs, simulations based on the following four controller designs are conducted:

1. The cooperatively tuned formation controller design (CTFC) that uses (12) as the weight tuning law. The control input is chosen as $u_i = \bar{\mathcal{S}}(u_{c,i}, \bar{\tau}_i, \bar{\psi}_i)$, where $u_{c,i} = \widehat{g}_i^{-1}(\dot{x}_{di} - \widehat{E}_i - k_i e_{xi})$, $\bar{\tau}_i = 0.24$ and $\bar{\psi}_i = 0.01$.

Table 1 Model parameters and initial states

Robot number	Model parameters		Initial states					
	R_i(m)	$\widehat{R}_i$(m)	p_i^x(m)	p_i^y(m)	θ_i(rad)	$\widehat{p}_i^x$(m)	$\widehat{p}_i^y$(m)	$\widehat{\theta}_i$(rad)
1	0.24	0.21	−0.2	−0.7	$-\pi/4$	0	−0.3	$-\pi/5$
2	0.23	0.25	1.6	3.6	$-\pi/5$	1.4	3.3	$-\pi/6$
3	0.30	0.33	−4	−2.4	$\pi/3$	−3.7	−2.1	$\pi/4$
4	0.28	0.24	−1.9	−1.1	$\pi/4$	−1.6	−0.8	$\pi/6$
5	0.25	0.28	−1.6	−4.6	$-\pi/3$	−1.1	−4.1	$-\pi/4$
6	0.32	0.29	3.6	−1.5	$-\pi/6$	3.9	−1.9	$-\pi/5$

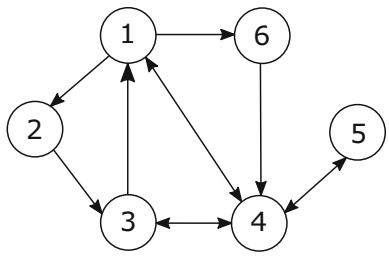

Fig. 3 A strongly connected topology for the multi-robot system

2. The restricted cooperatively tuned formation controller design (RCTFC) that uses (12) as the weight tuning law. The control input is chosen as $u_i = \bar{\mathcal{S}}(u_{c,i}, \bar{\tau}_i, \bar{\psi}_i)$, where $u_{c,i} = u_{m,i} + u_{e,i}$, $E_M = 0.10$, $\bar{\tau}_i = 0.24$ and $\bar{\psi}_i = \psi_E = 0.01$.
3. The observer-based formation controller design (OBFC) that implements the proposed neural-based observer (19) and the weight tuning law (20). Algorithm 1 is not applied and the controller is chosen as $u_i = \bar{\mathcal{S}}(u_{o,i}, \bar{\tau}_i, \bar{\psi}_i)$, where we have $u_{o,i} = u_{e,i} + \bar{\mathcal{S}}(u_{m,i}, \tau_i, \psi_i)$, $\bar{\tau}_i = 0.24$, $\tau_i = 0.22$, $E_M = 0.10$ and $\psi_i = \psi_E = \bar{\psi}_i = 0.01$.
4. The algorithm-and-observer-based formation controller design (AOBFC) that has the neural-based observer (19) tuned by (20). Algorithm 1 is implemented to generate the shrinking factor ξ_i and the controller is designed as (29), where $\tau_i = 0.22$, $E_M = 0.10$ and $\psi_E = \psi_u = 0.01$.

The tuning parameters of the NN are chosen as $\eta_1 = 15$, $\eta_2 = 0.1$, $\eta_3 = 0.1$ and $\eta_4 = 0.06$ in all simulations. Initially, $\widehat{J}_i(0)$ is chosen as a random 6×5 matrix with elements whose norms are less than 1 and $\widehat{W}_i(0)$ is chosen as a 5×3 zero matrix. For the designs that employ the neural-based observer (19), the parameters are chosen as $\beta_i = 0.9$ and $\gamma_i = \text{diag}\{12, 12, 18\}$.

The proportional parameter k_i in $u_{e,i}$ is chosen as $k_i = \bar{k} = 3$ for every agent in each simulation. To compare the performance of different designs, we define the 2-norm calculation of an arbitrary column vector $\mathcal{V}$ as $\bar{\Delta}(\mathcal{V}) = \sqrt{\mathcal{V}^{\mathrm{T}}\mathcal{V}}$. To illustrate the merits of using the neural-based observer (Theorem 2) over using the cooperative tuning approach (Theorem 1), we have provided the trends of $\bar{\Delta}(\widetilde{E})$, $\bar{\Delta}(e_x)$, $\bar{\Delta}(\delta_x)$ and $\bar{\Delta}(u)$ in Fig. 4. The SGUUB region and convergence time of each method are recorded in Table 2.

Although the norm of e_x and δ_x are both SGUUB for CTFC, we can hardly say that the system error states converged due to the high value of $b_{\widetilde{E}}$ (over 1000). Adding an extra smooth projection function to restrict the amplitudes of the NN output can lead to a success converge for both e_x and δ_x in RCTFC, but the accuracy of the NN is far from sufficient ($\bar{\Delta}(\widetilde{E}) \geq 100$). Furthermore, the control input of the RCTFC is also filled with chattering (see $\bar{\Delta}(u)$ in Fig. 4), which indicates that the cooperative tuning method (12) is not suitable when the actuators are restricted by saturation phenomenon.

On the contrary, $\bar{\Delta}(\widetilde{E})$ of the neural-based observer (19) in AOBFC is bounded within the region of 0.053 in 4.2 seconds, which proves the validity of the finite-time characteristics claimed in Theorem 2. Besides, the local formation tracking error e_x and the reference tracking error δ_x are SGUUB within 0.015 and 0.005, respectively. As a result, the existence of Problem 1 and the validity of Theorem 2 are both illustrated. Hence, the neural-based observer design (19) is a method more suitable than the cooperative tuning design (12) for systems with actuator saturation.

To verify the existence of the reverse effect mentioned in Problem 2, the values of each agent's local

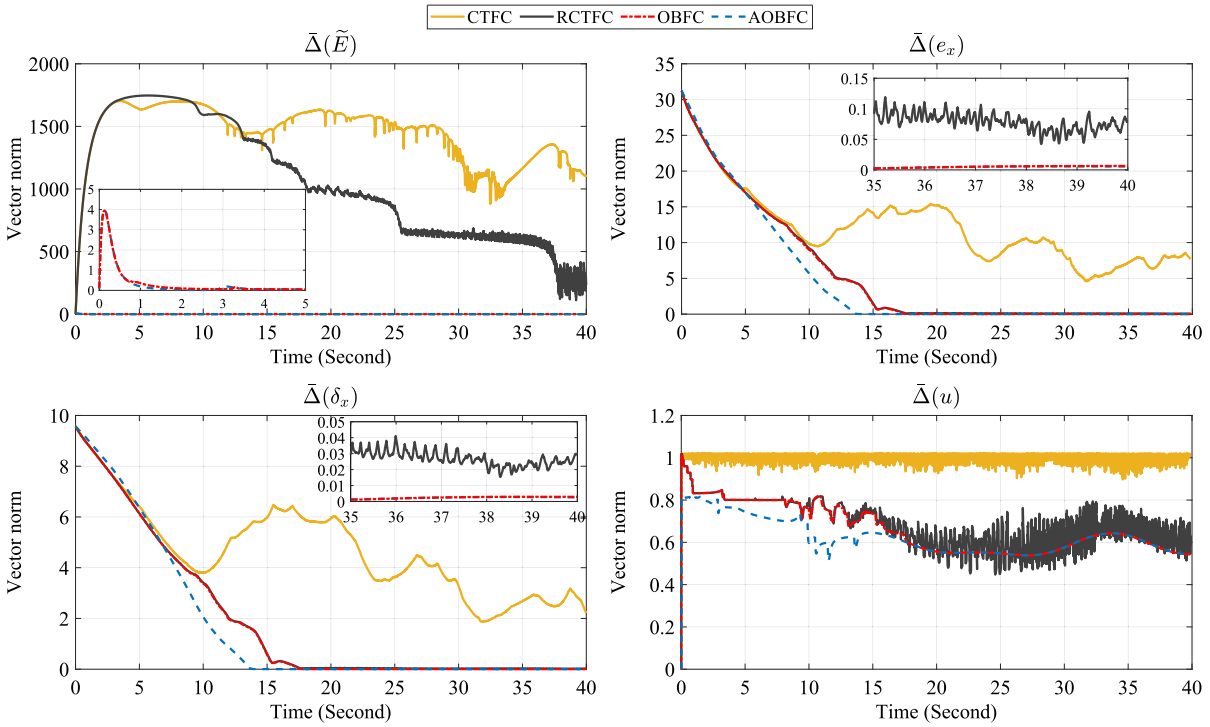

Fig. 4 Merits of using the neural-based observer over using the cooperative tuning design

Table 2 Performance comparison of four control schemes

Design	SGUUB region				Convergence time			
	$b_{\tilde{E}}$	b_{e_x}	b_{δ_x}	b_u	$t_{\tilde{E}}$	t_{e_x}	t_{δ_x}	t_u
CTFC	1.4×10^{3}	8.5	3.1	1.1	–	–	–	–
RCTFC	4.2×10^{2}	1.5×10^{-1}	5.5×10^{-2}	8.0×10^{-1}	37.7 s	17.6 s	17.6 s	10.1 s
OBFC	4.8×10^{-2}	1.5×10^{-2}	5.0×10^{-3}	6.5×10^{-1}	13.2 s	16.0 s	17.8 s	17.0 s
AOBFC	5.3×10^{-2}	1.5×10^{-2}	5.0×10^{-3}	6.5×10^{-1}	4.2 s	14.0 s	14.3 s	10.0 s

formation tracking error e_{xi} in the first 20 seconds are recorded and presented in Fig. 5. It is observed that every agent with the OBFC design experiences oscillation in the value of e_θ and part of the agents have fluctuated trends in e_x (agents 1, 3, 4 and 6) and e_y (agents 2, 5 and 6), which indicates the existence of the reverse effect. In comparison, most of the state fluctuations are attenuated in the AOBFC design. To validate that the CIDA is also capable to restrict the amplitudes of the control input within the saturation limit to satisfy $\mathcal{S}_i(\bar{u}_i) = \bar{u}_i$, the curves of each agent's control input are shown in Fig. 6.

The evolution of the shrinking factor ξ_i in Algorithm 1 is provided in Fig. 7, where we see that each ξ_i converges to 1 within the finite time of 13.8 seconds, illustrating the validity of Theorem 3. However, the proposed CIDA design cannot completely avoid the state fluctuation led by the reverse effect mentioned in Problem 2 (see agent 3 in Fig. 5). As we stated in the proof of Theorem 3, the factor ξ_i is determined by both the accessible control input amplitude $\bar{U}_{Mi}$ and the maximum error amplitude in e_{xi}. Hence, when one channel (p_i^y channel in e_{x3}) has a significant amount of error over other channels (p_i^x channel in e_{x3}), the channels with small error amplitudes can be overshadowed due to a low value of ξ_i, which leads to an increment of e_x. This circumstance is eased when the amplitude of different channels in the error vector achieves similar

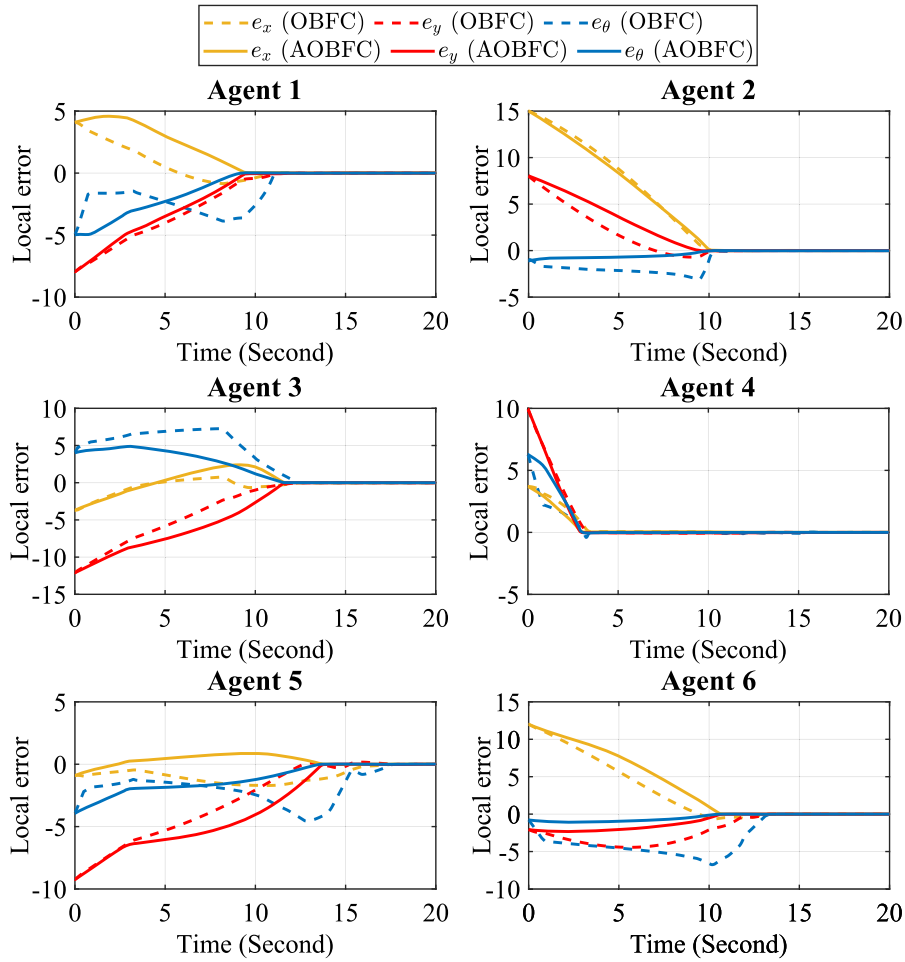

Fig. 5 Illustration of the reverse effect and the merits of implementing CIDA

values or the shrinking factor ξ_i rises to higher values (see agent 3 in Figs. 5 , 7 around 10 seconds).

To monitor the formation tracking behaviour of the system (4), the trajectories of all agents are recorded in Fig. 8. It is observed that the entire system is able to track the desired time-varying circular formation (34) (a circular formation whose centre is moving in a circular trajectory) with the existence of model uncertainty, external disturbances and actuator saturation, which concludes the effectiveness of the proposed formation control scheme (29) and the CIDA (Algorithm 1).

Remark 6 In all simulations, the system uncertainty is chosen as (34), which is a function related to both the system state x_i and the task time t. In practice, the relationship between the actual system state x_i and the task time t should be a continuous but unknown function $x_i = \mathcal{F}(t)$. In theory, we can also express the task time t with system state x_i by an unknown function $t = \mathcal{G}(x_i)$. Hence, both the system uncertainty $\bar{w}_i$ and the overall system uncertainty E_i can be treated as an unknown function that use x_i as the variable, which indicates that the estimation process (6) is valid.

5 Conclusion

In this paper, we focused on the implementation of three-layer NNs in the formation tracking problem of uncertain and saturated first-order multi-agent systems. First, a fully local-error-related cooperative tuning law for unsaturated agents was proposed to avoid the divergence of estimation error. After introducing the actuator saturation phenomenon along with the input coupling phenomenon into the system dynamics, two correlated problems including the slow convergence of cooperative neural estimation and the reverse effect were dis-

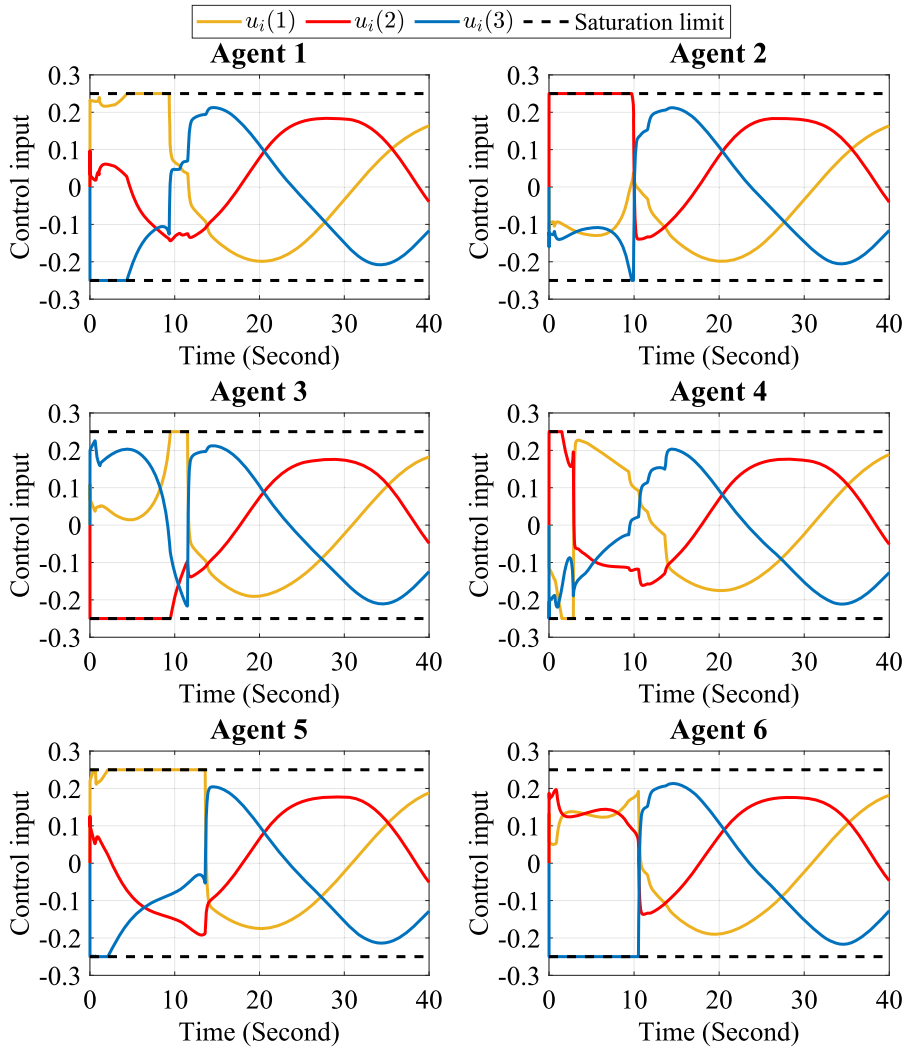

Fig. 6 Evolution of control inputs in AOBFC

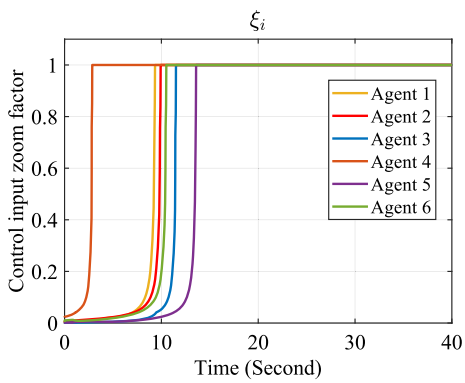

Fig. 7 Shrinking factor ξ_i

cussed. The three-layer NN was further modified into an observer to achieve semi-global finite-time convergence regardless of each agent's formation tracking error. A control input distribution algorithm was then developed to attenuate the reverse effect caused by coupled and saturated control inputs. Simulation examples are given to show the effectiveness and advantages of the proposed new designs compared with some existing results.

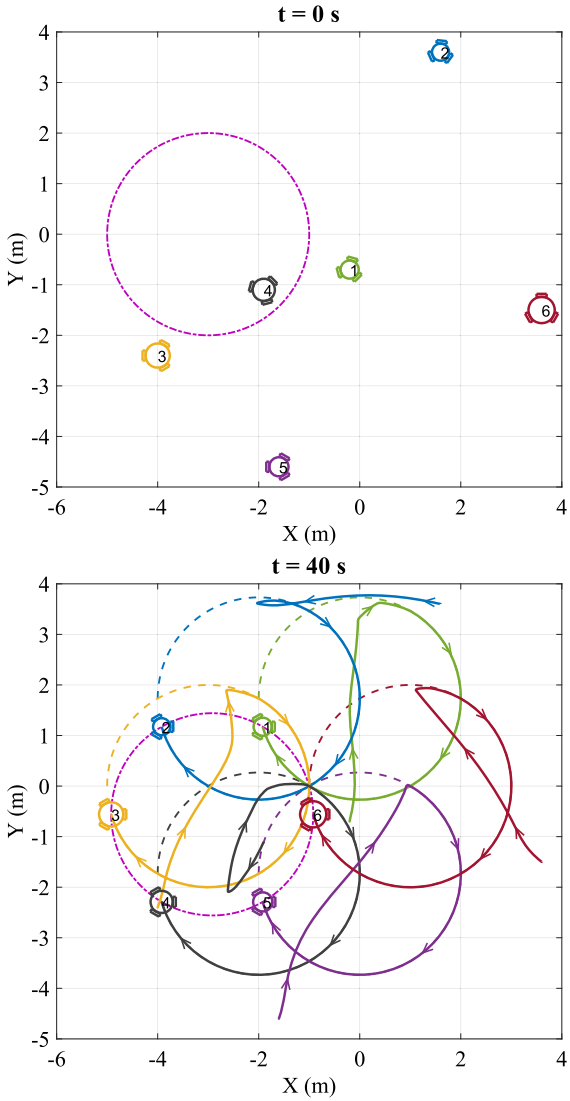

Fig. 8 Trajectories of the multi-robot system

Funding Open Access funding enabled and organized by CAUL and its Member Institutions.

Data Availability The data that support the findings of this study are available from the corresponding author upon reasonable request.

Declarations

Conflict of interest The authors declare that they have no conflict of interest.

References

1. Bai, W., Zhou, Q., Li, T., Li, H.: Adaptive reinforcement learning neural network control for uncertain nonlinear system with input saturation. IEEE Trans. Cybernet. **50**(8), 3433–3443 (2019)
2. De Tommasi, G., Lui, D.G., Petrillo, A., Santini, S.: A l_2-gain robust PID-like protocol for time-varying output formation-containment of multi-agent systems with external disturbance and communication delays. IET Control Theory & Appl. **15**(9), 1169–1184 (2021)
3. Dong, X., Hua, Y., Zhou, Y., Ren, Z., Zhong, Y.: Theory and experiment on formation-containment control of multiple multirotor unmanned aerial vehicle systems. IEEE Trans. Autom. Sci. Eng. **16**(1), 229–240 (2018)
4. Elhaki, O., Shojaei, K.: Neural network-based target tracking control of underactuated autonomous underwater vehicles with a prescribed performance. Ocean Eng. **167**, 239–256 (2018)
5. Fei, Y., Shi, P., Lim, C.C.: Neural network adaptive dynamic sliding mode formation control of multi-agent systems. Int. J. Syst. Sci. **51**(11), 2025–2040 (2020)
6. Fei, Y., Shi, P., Lim, C.C.: Robust and collision-free formation control of multiagent systems with limited information. IEEE Trans. Neural Netw. Learn. Syst. (2021). https://doi.org/10.1109/TNNLS.2021.3112679
7. Fei, Y., Shi, P., Lim, C.C.: Robust formation control for multi-agent systems: a reference correction based approach. IEEE Trans. Circuits Syst. I Regul. Pap. **68**(6), 2616–2625 (2021)
8. Fu, M., Yu, L.: Finite-time extended state observer-based distributed formation control for marine surface vehicles with input saturation and disturbances. Ocean Eng. **159**, 219–227 (2018)
9. Gao, W., Selmic, R.R.: Neural network control of a class of nonlinear systems with actuator saturation. IEEE Trans. Neural Netw. **17**(1), 147–156 (2006)
10. Ge, S.S., Hang, C.C., Lee, T.H., Zhang, T.: Stable adaptive neural network control, vol. 13. Springer Science & Business Media (2013)
11. Hu, Q., Jiang, B.: Continuous finite-time attitude control for rigid spacecraft based on angular velocity observer. IEEE Trans. Aerosp. Electron. Syst. **54**(3), 1082–1092 (2017)
12. Huang, X., Zhang, C., Lu, H., Li, M.: Adaptive reaching law based sliding mode control for electromagnetic formation flight with input saturation. J. Franklin Inst. **353**(11), 2398–2417 (2016)

13. Kim, Y.H., Lewis, F.L.: Neural network output feedback control of robot manipulators. IEEE Trans. Robot. Autom. **15**(2), 301–309 (1999)
14. Lewis, F.L., Zhang, H., Hengster-Movric, K., Das, A.: Cooperative control of multi-agent systems: optimal and adaptive design approaches. Springer Science & Business Media (2013)
15. Li, J., Du, J., Chang, W.J.: Robust time-varying formation control for underactuated autonomous underwater vehicles with disturbances under input saturation. Ocean Eng. **179**, 180–188 (2019)
16. Li, X., Shi, P.: Cooperative fault-tolerant tracking control of heterogeneous hybrid-order mechanical systems with actuator and amplifier faults. Nonlinear Dyn. **98**(1), 447–462 (2019)
17. Li, X., Shi, P., Wang, Y.: Distributed cooperative adaptive tracking control for heterogeneous systems with hybrid nonlinear dynamics. Nonlinear Dyn. **95**(3), 2131–2141 (2019)
18. Li, X., Shi, P., Wang, Y., Wang, S.: Cooperative tracking control of heterogeneous mixed-order multiagent systems with higher-order nonlinear dynamics. IEEE Trans. Cybernet. (2020). https://doi.org/10.1109/TCYB.2020.3035260
19. Liu, D., Huang, Y., Wang, D., Wei, Q.: Neural-network-observer-based optimal control for unknown nonlinear systems using adaptive dynamic programming. Int. J. Control **86**(9), 1554–1566 (2013)
20. Liu, X., Xiao, J.W., Chen, D., Wang, Y.W.: Dynamic consensus of nonlinear time-delay multi-agent systems with input saturation: an impulsive control algorithm. Nonlinear Dyn. **97**(2), 1699–1710 (2019)
21. Liu, Y., Shi, P., Yu, H., Lim, C.C.: Event-triggered probability-driven adaptive formation control for multiple elliptical agents. IEEE Trans. Syst. Man, and Cybernet.: Syst. **52**(1), 645–654 (2022)
22. Loizou, S., Lui, D.G., Petrillo, A., Santini, S.: Connectivity preserving formation stabilization in an obstacle-cluttered environment in the presence of time-varying communication delays. IEEE Trans. Autom. Control (2021). https://doi.org/10.1109/TAC.2021.3119003
23. Lu, N., Sun, X., Zheng, X., Shen, Q.: Command filtered adaptive fuzzy backstepping fault tolerant control against actuator fault. ICIC Exp. Lett. **15**(4), 357–365 (2021)
24. Lui, D.G., Petrillo, A., Santini, S.: Distributed model reference adaptive containment control of heterogeneous multiagent systems with unknown uncertainties and directed topologies. J. Franklin Inst. **358**(1), 737–756 (2021)
25. Park, B.S., Yoo, S.J.: Connectivity-maintaining and collision-avoiding performance function approach for robust leader-follower formation control of multiple uncertain underactuated surface vessels. Automatica **127**, 109501 (2021)
26. Ren, W., Beard, R.W.: Consensus seeking in multiagent systems under dynamically changing interaction topologies. IEEE Trans. Autom. Control **50**(5), 655–661 (2005)
27. Shi, P., Yu, J.: Dissipativity-based consensus for fuzzy multiagent systems under switching directed topologies. IEEE Trans. Fuzzy Syst. **29**(5), 1143–1151 (2021)
28. Shojaei, K.: Neural network formation control of underactuated autonomous underwater vehicles with saturating actuators. Neurocomputing **194**, 372–384 (2016)
29. Tsai, C.C., Wu, H.L., Tai, F.C., Chen, Y.S.: Distributed consensus formation control with collision and obstacle avoidance for uncertain networked omnidirectional multi-robot systems using fuzzy wavelet neural networks. Int. J. Fuzzy Syst. **19**(5), 1375–1391 (2017)
30. Wang, C., Tnunay, H., Zuo, Z., Lennox, B., Ding, Z.: Fixed-time formation control of multirobot systems: Design and experiments. IEEE Trans. Industr. Electron. **66**(8), 6292–6301 (2019)
31. Wu, L.B., Park, J.H., Xie, X.P., Ren, Y.W., Yang, Z.: Distributed adaptive neural network consensus for a class of uncertain nonaffine nonlinear multi-agent systems. Nonlinear Dyn. **100**(2), 1243–1255 (2020)
32. Xiong, S., Hou, Z.: Data-driven formation control for unknown MIMO nonlinear discrete-time multi-agent systems with sensor fault. IEEE Trans. Neural Netw. Learn. Syst. (2021). https://doi.org/10.1109/TNNLS.2021.3087481
33. Yan, B., Shi, P., Lim, C.C.: Robust formation control for nonlinear heterogeneous multiagent systems based on adaptive event-triggered strategy. IEEE Trans. Autom. Sci. Eng. (2021). https://doi.org/10.1109/TASE.2021.3103877
34. Yang, R., Liu, L., Feng, G.: Cooperative output tracking of unknown heterogeneous linear systems by distributed event-triggered adaptive control. IEEE Trans. Cybernet. **52**(1), 3–15 (2022)
35. Yu, D., Dong, L., Yan, H.: Adaptive sliding mode control of multi-agent relay tracking systems with disturbances. J. Control and Decision **8**(2), 165–174 (2021)
36. Zhang, J., Lyu, M., Shen, T., Liu, L., Bo, Y.: Sliding mode control for a class of nonlinear multi-agent system with time delay and uncertainties. IEEE Trans. Industr. Electron. **65**(1), 865–875 (2017)
37. Zhang, L., Chen, M., Wu, B.: Observer-based controller design for networked control systems with induced delays and data packet dropouts. ICIC Exp. Lett. Part B: Appl. **12**(3), 243–254 (2021)
38. Zhang, Z., Yang, P., Hu, X., Wang, Z.: Sliding mode prediction fault-tolerant control of a quad-rotor system with multi-delays based on icoa. Int. J. Innovative Comput. Inform. Control **17**(1), 49–66 (2021)
39. Zhao, Y., Hao, Y., Wang, Q., Wang, Q., Chen, G.: Formation of multi-agent systems with desired orientation: a distance-based control approach. Nonlinear Dyn. (2021). https://doi.org/10.1007/s11071-021-06948-5
40. Zheng, S., Shi, P., Wang, S., Shi, Y.: Adaptive neural control for a class of nonlinear multiagent systems. IEEE Trans. Neural Netw. Learn. Syst. **32**(2), 763–776 (2020)